THE JOURNAL OF BIOLOGICAL CHEMISTRY
Vol. 279, No. 3, Issue of January 16, pp. 1627–1636, 2004

*Printed in U.S.A.*

# Conserved High Affinity Ligand Binding and Membrane Association in the Native and Refolded Extracellular Domain of the Human Glycine Receptor α1-Subunit*

Received for publication, April 11, 2003, and in revised form, October 16, 2003
Published, JBC Papers in Press, October 30, 2003, DOI 10.1074/jbc.M303811200

**Ulrike Breitinger‡, Hans-Georg Breitinger‡, Finn Bauer§, Karim Fahmy¶, Daniela Glockenhammer‡, and Cord-Michael Becker‡‖**

*From the ‡Institut für Biochemie, Emil-Fischer-Zentrum, Friedrich-Alexander-Universität Erlangen-Nürnberg, D-91054 Erlangen, Germany, the §Lehrstuhl Biopolymere, Universität Bayreuth, D-95440 Bayreuth, Germany, and the ¶Institut für Kern- und Hadronenphysik, Forschungszentrum Rossendorf, D-01314 Dresden, Germany*

**The strychnine-sensitive glycine receptor (GlyR) is a ligand-gated chloride channel composed of ligand binding α- and gephyrin anchoring β-subunits. To identify the secondary and quaternary structures of extramembraneous receptor domains, the N-terminal extracellular domain (α1-(1–219)) and the large intracellular TM3–4 loop (α1-(309–392)) of the human GlyR α1-subunit were individually expressed in HEK293 cells and in *Escherichia coli*. The extracellular domain obtained from *E. coli* expression was purified in its denatured form and refolding conditions were established. Circular dichroism and Fourier-transform-infrared spectroscopy suggested ~25% α-helix and ~48% β-sheet for the extracellular domain, while no α-helices were detectable for the TM3–4 loop. Size exclusion chromatography and sucrose density centrifugation indicated that isolated glycine receptor domains assembled into multimers of distinct molecular weight. For the extracellular domain from *E. coli*, we found an apparent molecular weight compatible with a 15mer by gel filtration. The N-terminal domain from HEK293 cells, analyzed by sucrose gradient centrifugation, showed a bimodal distribution, suggesting oligomerization of ~5 and 15 subunits. Likewise, for the intracellular domain from *E. coli*, a single molecular mass peak of ~49 kDa indicated oligomerization in a defined native structure. As shown by [$^3$H]strychnine binding, expression in HEK293 cells and refolding of the isolated extracellular domain reconstituted high affinity antagonist binding. Cell fractionation, alkaline extraction experiments, and immunocytochemistry showed a tight plasma membrane association of the isolated GlyR N-terminal protein. These findings indicate that distinct functional characteristics of the full-length GlyR are retained in the isolated N-terminal domain.**

The inhibitory glycine receptor (GlyR)[1] is a neurotransmitter-gated ion channel, mediating rapid synaptic transmission in the central nervous system (1–3). The GlyR is a member of the ligand-gated ion channel superfamily, which also includes the nicotinic acetylcholine receptor (nAChR), serotonin 5-HT$_3$ receptor, as well as GABA$_{A/C}$ receptors. Members of this protein family share a quaternary structure of five subunits surrounding a central ion-conducting pore (4–6). The GlyR isoform prevalent in adult mammalian central nervous system is thought to comprise three α1-subunits and two structural β-subunits, which are thought to contribute to synaptic anchoring of receptor complexes. Generally, GlyR α-subunits possess the ability to form functional homomeric receptor channels. The subunit topology of the nAChR superfamily, as deduced from hydropathy analysis, consists of a large N-terminal extracellular domain, followed by four hydrophobic stretches of sufficient length to span the plasma membrane, and the extracellular C terminus (7). Of all transmembrane regions, TM2 forms the inner lining of the central ion channel. A large cytosolic loop, flanked by TM3 and TM4, is thought to mediate intracellular interactions. Based on NMR studies of corresponding synthetic peptides, TM2 of the nAChR and GlyR has been demonstrated to be α-helical (8, 9). Several attempts have been made to elucidate the structure of the nAChR extracellular domain, which is widely seen as a prototype of the structural homologous GlyR. Recently, the chicken α7 extracellular domain was expressed in *Xenopus* oocytes (10), while a soluble fusion protein of the rat α7 nAChR N-terminal domain and maltose binding protein has been generated in *Escherichia coli* (11). In addition, the extracellular domain from the human muscle AChR α subunit was expressed as a soluble protein in the yeast *Pichia pastoris* (12), while the α7 nAChR extracellular domain fused to GST was expressed in *E. coli* and subsequently refolded (13). In an alternative approach, the x-ray structure of a molluscan ACh binding protein was solved at atomic resolution (14), and revealed structural similarity to the extracellular domain of nAChRs, as determined by electron microscopy (15).

The extracellular domain of the GlyR α1-subunit comprises ~50% of the entire subunit sequence, and contains determinants of ligand binding and subunit assembly (16). Six of eight key residues that form the putative intersubunit contact surface are located within the stretch of amino acid residues 1 to 100 (17), a segment that was not associated with high affinity ligand binding (18). Site-directed mutagenesis studies suggest that glycine and strychnine bind to distinct, but overlapping,

* This work was supported by the Deutsche Forschungsgemeinschaft (SFB 353) and Fonds der Chemischen Industrie. The costs of publication of this article were defrayed in part by the payment of page charges. This article must therefore be hereby marked "*advertisement*" in accordance with 18 U.S.C. Section 1734 solely to indicate this fact.

‖ To whom correspondence should be addressed: Institut für Biochemie, Emil-Fischer-Zentrum, Universität Erlangen-Nürnberg, Fahrstrasse 17, D-91054 Erlangen, Germany. Tel.: 49-9131-85-24190; Fax: 49-9131-85-22485; E-mail: cmb@biochem.uni-erlangen.de.

[1] The abbreviations used are: GlyR, glycine receptor; PEI, polyethyleneimine; ATR, attenuated total reflection; FTIR, Fourier-transform-infrared; CHAPS, 3-[(3-cholamidopropyl)dimethylammonio]-1-propanesulfonic acid; GST, glutathione *S*-transferase; DORA, dot blot receptor assay; TM, transmembrane; mAb, monoclonal antibody; HEK, human embryonic kidney.

sites on recombinant receptors (16). In the GlyR $\alpha$1-subunit, residues Ala$^{101}$-Asn$^{102}$, Gly$^{160}$-Tyr$^{161}$, Lys$^{193}$, and Lys$^{200}$-Thr$^{204}$ represent determinants of ligand binding and agonist-antagonist discrimination. Recently, an alternative model of the GlyR topology was proposed, based on limited proteolysis and chemical modification of reconstituted $\alpha$1 GlyR (19). In particular, this alternative model suggested the presence of one or more membrane-associated stretches within the postulated extracellular N-terminal domain as well as a new topology of TM1 and TM3.

Here, we describe the large scale recombinant expression and purification of the isolated GlyR $\alpha$1 extracellular and intracellular domains. Strychnine affinity in the nanomolar range was retained for both, eukaryotic and refolded N-terminal domains. Surprisingly, the isolated extracellular domain showed a strong membrane association when expressed in HEK293 cells. Secondary structure analysis suggested a significant contribution of $\alpha$-helices to the extracellular domain, while no $\alpha$-helical structure was detectable in the intracellular TM3–4 loop. Our results show that other extracellular regions of the GlyR, such as the TM2–3 loop and the C terminus may be important for signal transduction and channel gating (16, 42), but are not essential for ligand binding.

## EXPERIMENTAL PROCEDURES

*Construction of Vectors, Expression, and Purification of Fusion Proteins*—Domains of interest were amplified by PCR using hs$\alpha$1 DNA as template. Oligonucleotides were custom-synthesized (Invitrogen, Karlsruhe, Germany). PCR primers contained appropriate restriction sites, allowing ligation into the pET30a (Novagen, Darmstadt, Germany) and pRK5 vectors. Successful mutations were verified by DNA sequencing (ABI Systems, Weiterscheidt, Germany). After transformation and expression, BL21 cells (Novagen, Darmstadt, Germany) were harvested by centrifugation, resuspended in 50 mM Tris-HCl, 2.5 mM EDTA, pH 7.4, treated with lysozyme (0.1 mg/ml, 30 min, 0 °C) and sonicated (eight 10-s pulses) on ice. Sonification was repeated and the supernatant collected for native purification. For purification under denaturing conditions, the pellet was washed four times with 50 mM Tris-HCl, 2.5 mM EDTA, 0.5% Triton X-100, pH 8.2, and finally dissolved in 100 mM $NaP_i$, 10 mM Tris-HCl, 8 M urea, pH 8.0. The denatured protein was applied to a Ni-agarose column (Qiagen, Hilden, Germany), washed at pH 5.9 and eluted at pH 4.5. Native purification, performed on a Ni-agarose column, was achieved by washing and eluting with increasing imidazole concentrations. To avoid precipitation of these protein constructs in the presence of protease substrate buffers, tags were not removed.

*Refolding*—A variety of folding conditions was tested, following published folding screens (20, 21). After 2 h of incubation in denaturing buffer, 10 $\mu$l of the dissolved inclusion bodies (1 mg/ml) were added to 990 $\mu$l of folding screen solution. Samples were incubated overnight at 4 °C, dialyzed for 6 h against 100 ml of proteolysis buffer (20 mM Tris-HCl, pH 8.0), concentrated and proteolyzed using subtilisin (1 $\mu$g/ml). The reaction was stopped after 100 min by adding phenylmethylsulfonyl fluoride (1 mM), and the samples were vacuum-dried. Western blot analysis was carried out for refolded protein samples before and after proteolysis. Large scale preparations (20 ml of denatured protein solution, 2–5 mg/ml) were made by stepwise dialysis: a first dialysis step against 1 liter of a 1:1 mixture of folding buffer and denaturing buffer was followed by repeatedly exchanging 30% of the solution with fresh folding buffer every 3 h. This step was repeated six times, followed by a final dialysis against pure folding buffer overnight.

*Mass Spectrometry*—For matrix-assisted laser desorption ionization time of flight mass spectrometry (MALDI-TOF-MS) and surface enhanced laser desorption ionization (SELDI), protein samples were diluted to 2 mg/ml and mixed (1:1) with a CCA-Matrix (3-hydroxy-$\alpha$-cyano-cinnamic-acid; saturated solution in 30% acetonitrile/0.1% trifluoroacetic acid), dotted onto a steel target, and air-dried. MALDI-TOF-MS analysis was performed on an Autoflex spectrometer (Bruker Daltonics, Bremen, Germany) in the reflector mode while the SELDI analysis was carried out on a PBS II spectrometer (Ciphergen, Göttingen, Germany). Desorption of the samples was carried out using a nitrogen laser (337 nm). For the MALDI-TOF-MS analysis, the samples were accelerated with 19 kV after a delay of 3500 ns and several individual spectra of the respective samples were averaged. A peptide standard mix served as an external calibration. For SELDI analysis, time-of-flight spectra were generated by averaging 360 laser shots collected in the positive mode at laser intensity 259, detector sensitivity 10, and a focus lag time of 900 ns.

*Transfection of HEK 293 Cells, Alkaline Extraction, and Immunocytochemistry*—HEK293 cells were cultured and transfected, and crude membrane fractions were prepared as described (22). For Western blot analysis (23) the monoclonal antibody mAb4a, a mouse monoclonal His-tag antibody (Novagen, Darmstadt, Germany) or a mouse monoclonal gephyrin antibody (BD Sciences, Heidelberg, Germany) were used, followed by a Cy5-coupled goat anti-mouse antibody gdMIgG-Cy5 (Dianova, Hamburg, Germany), and visualized on a Storm 860 Fluoroimager (Molecular Dynamics, Krefeld, Germany). To test for membrane association, membrane preparations from transfected HEK293 cells (0.5 mg/ml) were incubated for 60 min at pH 7.4 or pH 11.0 at 4 °C and centrifuged (180,000 $\times$ *g*, 4 °C) for 90 min as described (24). The pellets and supernatants were then subjected to Western blot analysis. HEK293 cells, grown on cover slips, were transferred to a 24-well plate 2 days after transfection. After fixation in paraformaldehyde for 10 min, cover slips were washed twice in PBS (1.5 mM $KH_2PO_4$, 6.5 mM $Na_2HPO_4$, 3 mM KCl, 137 mM NaCl), and blocked with 5% sheep serum for 30 min. For permeabilization, cells were treated with 0.1% Triton X-100. Primary (mAb4a, anti-Gephyrin) and secondary antibody, Cy3 goat anti-mouse F(ab)$_2$ (Dianova, Hamburg, Germany) were applied for 60 min, every step followed by three washes with phosphate-buffered saline. Cover slips were transferred to slides and examined on a confocal microscope (Leica, Bensheim, Germany).

*[$^3$H]Strychnine Binding*—Different radioligand filtration assays were performed to determine [$^3$H]strychnine binding of soluble protein (i, ii) and membrane-associated protein (iii): (i) Polyethylene glycol (PEG) precipitation: 15 $\mu$g of refolded protein, 0.13% $\gamma$-globulin, [$^3$H]strychnine (PerkinElmer Life Sciences, Zaventem, Belgium; specific activity, 47.8 mCi/mol), and binding buffer B (25 mM $KP_i$ pH 7.4, 200 mM KCl) in the presence and absence of cold strychnine were incubated on ice for 30 min. PEG400 (15%) in buffer B was added and the mixture incubated on ice for another 30 min. The precipitated protein was applied to GF/C filter, soaked in 0.1% bovine serum albumin, and washed twice with cold buffer B. (ii) Adsorption on polyethyleneimine (PEI)-coated filters: Total cell extract preparation (50 $\mu$g) and [$^3$H]strychnine in the presence or absence of cold strychnine were incubated on ice for 30 min, before applying to 0.3% PEI-soaked GF/B filter and washing twice with buffer B. (iii) Filter adsorption of membrane fractions: Protein obtained from membrane preparations was treated as described previously (23). For all methods, dried filters were subjected to scintillation counting (Roth, Karlsruhe, Germany). Binding data were fitted to Equation 1.

$$dpm_{spec} = B_{\max} \frac{1}{1 + K_D/[Str]} \qquad \text{(Eq. 1)}$$

Here, $dpm_{spec}$ represents specific binding expressed as scintillator counts ($dpm_{spec}$ was determined by subtracting unspecific counts from total counts), $B_{\max}$ = total number of agonist binding sites, $K_D$ = binding constant, $[Str]$ = [$^3$H]strychnine concentration. For each concentration, unspecific binding was determined in the presence of 1 $\mu$M cold strychnine. Determinations were carried out in triplicate.

*Size Exclusion Chromatography and Sucrose Gradient Centrifugation*—Sephacryl S400 (30 ml) and Sephacryl S200 (120 ml) columns were chosen to determine the native molecular weight of the GlyR extra- and intracellular domains, respectively. Calibration runs of marker proteins (Amersham Biosciences) were performed in triplicate on a BioLogicHR FPLC station (BioRad, München, Germany). $K_{av}$ is defined by Equation 2,

$$K_{av} = \frac{V_e - V_o}{V_t - V_o} \qquad \text{(Eq. 2)}$$

where $V_e$ is the elution volume of the protein, $V_o$ is the column void volume, and $V_t$ is the total bed volume. Runs were performed at 4 °C in 50 mM $KP_i$ pH 7.4, 100 mM NaCl for Sephacryl S200 and 50 mM Tris-HCl, 50 mM NaCl for Sephacryl S400. For molecular weight determinations in a continuous sucrose gradient, 1 ml of total cell extract containing ~5 mg of protein was layered on a continuous 10–40% sucrose gradient (26 ml) in 25 mM Tris-HCl, pH 7.4, 25 mM NaCl, 1% Triton X-100 on top of a 60% sucrose cushion (3 ml). After centrifugation for 14 h in a Sorvall SW-28 rotor at 27,000 rpm GlyR antigen was quantified using a dot blot receptor assay (DORA).

Sucrose fractions (1.5 ml) were collected, and 300 μl of the fraction was taken up in 300 μl of uptake buffer (150 mM NaCl, 50 mM Tris-HCl, pH 7.4, 2% sodium desoxycholate, 40% methanol, 5 mM EDTA, 5 mM EGTA), and directly spotted onto a nitrocellulose membrane. GlyR content was then determined as described for Western blot analysis, mAb4a immune signal was quantified on a Storm860 fluoroimager. The following protein markers were used: cytochrome *c* (12.3 kDa, 1.83 Svedberg (S)), ovalbumin (43 kDa, 3.55 S), malate dehydrogenase (70 kDa, 4.32 S), lactic dehydrogenase (140 kDa, 6.95 S), and catalase (232 kDa, 11.3 S).

*CD Spectroscopy*—Purified intra- and extracellular GlyR domains, expressed in *E. coli* and buffered in 10 mM $KP_i$ pH 7.4, were subjected to CD analysis. Measurements were performed on a JASCO-J810 spectrometer (JASCO, Groβ-Umstadt, Germany) in a 0.1-cm analytical cell. All spectra were baseline corrected by subtracting buffer runs. Eight individual scans were taken at room temperature in a range of 320 to 180 or 200 nm, with a 0.5-nm step size and averaged. Protein concentrations were determined by measuring the absorbance at 280 nm using the equation $c = A_{280\ nm}/(\epsilon \times l)$. The path length l was 1 cm, the extinction coefficients (S_α1-(1–219), $\epsilon$ = 27550 $M^{-1}$ $cm^{-1}$; hsα1-(1–219), $\epsilon$ = 27550 $M^{-1}$ $cm^{-1}$; hsα1-(309–392), $\epsilon$ = 1400 $M^{-1}$ $cm^{-1}$) were calculated from the protein sequence (48). While α-helical structure elements give distinct CD spectra with negative maxima at 222 and 208 nm, spectra obtained from β-sheets have a broad negative maximum at 215 nm (25, 26). The left-handed type II polyproline (PPII) helix (26, 27) yields spectra with an intense negative band at 204 nm. Here, the α-helix content was estimated using single wavelength methods based on the maxima at 222 and 208 nm (28, 29). Additionally, a least square method was used to estimate secondary structure elements from a data base of reference CD spectra (30).

*ATR-FTIR Spectroscopy*—Attenuated total reflection (ATR) Fourier-transform-infrared (FTIR) spectroscopy was used to assess the relative amounts of secondary structure in the N-terminal extracellular domain and in the TM3–4 loop of the GlyR α1 subunit in aqueous solution. 20 μl of a solution containing 4–15 mg protein/ml in 10 mM sodium phosphate buffer pH 7.4 were placed on the silicon crystal of a Bruker Bio-ATR-II cell and 256 interferograms averaged at 2 $cm^{-1}$ resolution with a Bruker Vector 22 spectrometer. Absorption spectra were obtained from the transformed interferograms using the pH-matched buffer without protein as the reference. The amide I and II absorption bands were fitted by gaussian bands corresponding to known absorption maxima of secondary structure elements (31–33) using the Microcal Origin and OPUS software. The corresponding peak positions were restricted within 2 $cm^{-1}$ to the frequencies at which minima occurred in the second derivative of the original spectra. Band widths were restricted to 30–32 $cm^{-1}$. The integrals of the individual gaussian bands were taken as a relative measure of the type of secondary structure that corresponds with the center frequency of the resolved band.

## RESULTS

For analysis of GlyR α1-subunit extra- and intracellular domains, three different cDNA constructs were designed and expressed in both *E. coli* and in HEK293 cells. The vector pET30a, containing a variety of functional sites, was prepared for high yield protein expression in *E. coli*. In particular, a His-tag, a thrombin site, an S-tag (*i.e.* a 15-residue part of the ribonuclease S protein), and an enterokinase cleavage site preceded the fusion protein. To control for a potential interference with the S-tag, the truncated vector pET30aΔS-tag was designed, lacking the S-tag and the enterokinase cleavage site of the pET30a vector. The vector pRK5 was chosen for eukaryotic protein expression in HEK293 cells (34). Target proteins expressed in *E. coli* (pET30a and pET30aΔS-tag) included the extracellular domain without signal peptide and the large intracellular loop (Fig. 1, *constructs 1*, *2*, *6*). The influence of the His-tag on ligand binding was examined by expression of the extracellular domain in HEK293 cells (Fig. 1, *constructs 3* and *4*). Investigation of a potential membrane association of the isolated extracellular domain required a construct containing the signal peptide for incorporation into the plasma membrane compartments (Fig. 1, *construct 5*).

*Protein Expression, Purification, and Refolding of Pure GlyR Protein Constructs*—For large scale production of pure protein,

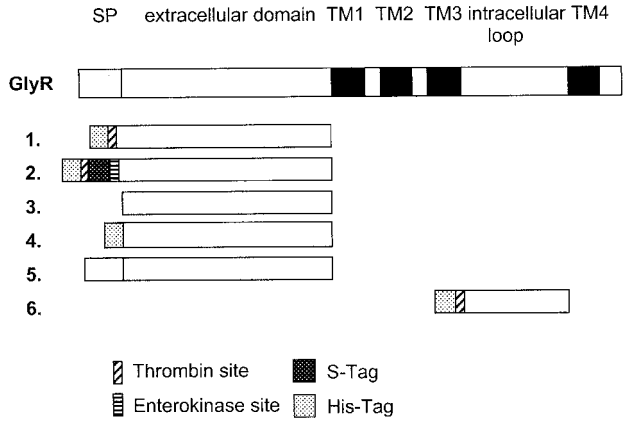


| Constructs | Vector | Name |
|---|---|---|
| 1. 6xHis hsα1(1-219) | pET30a ΔS-tag | *E.coli*_α1-(1-219) |
| 2. 6xHis-S-Tag hsα1(1-219) | pET30a | *E.coli*_S_α1-(1-219) |
| 3. hsα1(1-219) | pRK5 | HEK_α1-(1-219) |
| 4. 6xHis-hsα1(1-219) | pRK5 | HEK_His_α1-(1-219) |
| 5. SP-hsα1(1-219) | pRK5 | HEK_SP_α1-(1-219) |
| 6. 6xHis-hsα1(309-392) | pET30a ΔS-tag | *E.coli*_α1-(309-392) |

FIG. 1. **Human glycine receptor α1 constructs used in this study.** The signal peptide (*SP*) and transmembrane domains (*TM 1–4*) are indicated. The vector pET30a contained a His-tag, followed by a thrombin-site, an S-tag, an enterokinase-site, and the fusion protein. The vector pET30aΔS-tag lacked the S-tag and the following enterokinase-site. The extracellular domain was cloned into both vector variants (constructs 1 and 2), while the large intracellular loop (construct 6) was engineered in vector pET30aΔS-tag only. Constructs 3–5 are variants of the extracellular domain α1-(1–219) in the vector pRK5.

human GlyR α1 domains were expressed in *E. coli*. Initial affinity purification using maltose binding protein fused to the target protein proved to be ineffective due to degradation of the receptor polypeptide during factor Xa treatment (not shown). Therefore, a His-tagged fusion protein was engineered for recombinant expression, followed by purification on Ni-NTA agarose. When the large intracellular loop was expressed in *E. coli*, a soluble protein was obtained which was efficiently purified under native conditions using a Ni-agarose column. In contrast, *E. coli* expression of the extracellular domain almost exclusively resulted in inclusion body formation. As shown for other receptors, *e.g.* the N-terminal domain of the α7 AChR (13), proteins from inclusion bodies may properly refold, but the refolding procedure does not necessarily result in a high percentage of correctly folded protein (35). While we made considerable efforts to avoid inclusion body formation by testing different *E. coli* strains and varying the expression conditions, we never obtained sufficient amounts of the target protein in its soluble form (not shown). Nevertheless, expression in form of inclusion bodies yielded high amounts of almost pure N-terminal protein, which was further purified on a Ni-NTA column under denaturing conditions. Refolding conditions were established following a modified protocol of Heiring and Muller (21) (Table I). Since correctly folded protein is expected to be more stable against degradation than a non- or incorrectly folded structure, resistance to a protease digest served as an indicator of correct folding (21). Refolded protein, prepared by 100-fold dilution into folding buffer, therefore, was treated with subtilisin and subjected to Western blot analysis (Fig. 2). Proper protein refolding was assessed by comparing signal intensities of intact full-length protein and degradation products. Large scale preparation of pure protein was carried out by stepwise dialysis against refolding buffer. Under these conditions, best refolding was obtained with 50 mM Tris-HCl and 7 μM $CuCl_2$ (Fig. 2, *lane 16*). Several other conditions resulted in

TABLE I
*Refolding screen for the GlyR extracellular domain*

Formulations of the reagents: Tris-HCl, 55 mM, pH 8.2; MES, 50 mM, pH 6.5; salt high, 250 mM NaCl, 10 mM KCl; salt low, 10 mM NaCl, 0.5 mM KCl; EDTA, 1 mM; $MgCl_2/CaCl_2$, 2 mM $MgCl_2$, 2 mM $CaCl_2$; $CuCl_2$, 7 $\mu$M; PEG, 0.05% (w/v) PEG 4000, present (+) or absent (−); detergent, 0.3 mM $\beta$-lauryl maltoside (LM), no detergent (−); Chaotr., 0.5 M guanidine-HCl, present (+) or absent (−); sucrose, 0.5 M; arginine, (arg) 0.55 M; dithiothreitol (DTT), 1 mM; GSSG/GSH, 0.1 mM oxidized glutathione (GSSG), 1 mM reduced glutathione (GSH).

| No. | Buffer | Salt | Cation/no cation | PEG | Detergent | Chaotr. | Polar/non polar addit. | Redox comp. |
|---|---|---|---|---|---|---|---|---|
| 1 | Tris-HCl | High | EDTA | + | – | – | – | DTT |
| 2 | MES | Low | Mg-/$CaCl_2$ | – | LM | + | – | GSSG/GSH |
| 3 | MES | Low | EDTA | + | – | + | Sucr/arg | GSSG/GSH |
| 4 | Tris-HCl | High | Mg-/$CaCl_2$ | – | LM | – | Sucr/arg | DTT |
| 5 | Tris-HCl | High | Mg-/$CaCl_2$ | + | LM | + | Sucr/arg | GSSG/GSH |
| 6 | Tris-HCl | Low | EDTA | + | LM | + | Sucrose | DTT |
| 7 | Tris-HCl | Low | Mg-/$CaCl_2$ | – | – | + | Arginine | DTT |
| 8 | MES | High | EDTA | + | LM | – | Arginine | GSSG/GSH |
| 9 | MES | High | Mg-/$CaCl_2$ | + | – | + | Sucrose | DTT |
| 10 | Tris-HCl | Low | EDTA | – | LM | – | Sucrose | GSSG/GSH |
| 11 | Tris-HCl | Low | Mg-/$CaCl_2$ | + | – | – | Arginine | GSSG/GSH |
| 12 | MES | High | EDTA | – | LM | + | Arginine | DTT |
| 13 | Tris-HCl | High | EDTA | – | – | + | – | GSSG/GSH |
| 14 | MES | Low | Mg-/$CaCl_2$ | + | LM | – | – | DTT |
| 15 | MES | Low | EDTA | – | – | – | Sucr/arg | DTT |
| 16 | Tris-HCl | – | $CuCl_2$ | – | – | – | – | – |

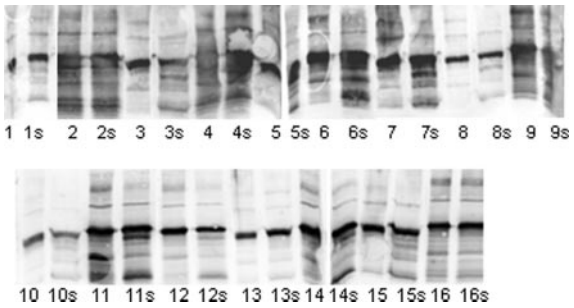


FIG. 2. **Western blot analysis of results obtained from refolding assays.** Refolded proteins (folding conditions 1–16) before (*X*) and after (*Xs*) subtilisin treatment are shown.

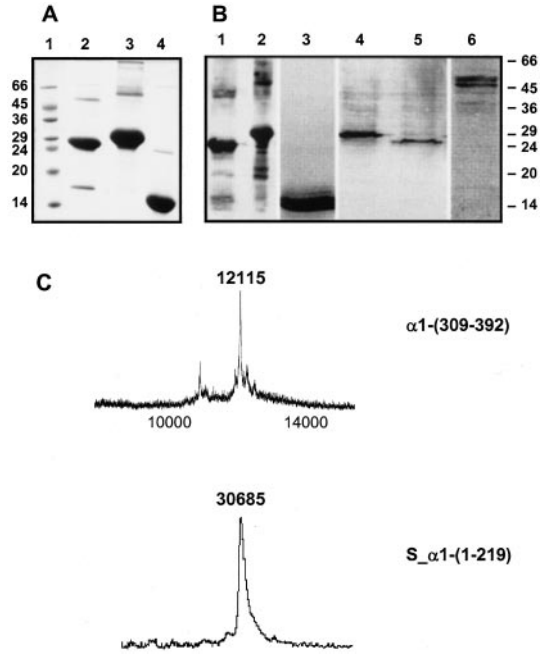


FIG. 3. **Purification and verification of GlyR constructs.** *A*, Coomassie gel of purified proteins: *lane 1*, SDS-7 low molecular weight markers (Sigma); *lane 2*, *E. coli*_α1-(1–219), refolded; *lane 3*, *E. coli*-S_α1-(1–219), refolded; *lane 4*, *E. coli*_α1-(309–392). *B*, Western blot analysis (mAb4a): *lane 1*, *E. coli*_α1-(1–219), refolded; *lane 2*, *E.coli*-S_α1-(1–219), refolded; *lane 3*, *E. coli*_α1-(309–392); *lane 4*, HEK-His_α1-(1–219), total cell extract; *lane 5*, HEK_α1-(1–219), total cell extract; *lane 6*, HEK_hsα1, total cell extract. *C*, SELDI and MALDI-TOF-MS analyses verifying the molecular masses of the extracellular domain S_α1-(1–219) and the TM3–4 loop α1-(309–392), respectively.

efficient refolding during the initial test analysis (Fig. 2, *lanes 8*, *12*, and *13*), but were hampered by precipitation of the desired protein during final large-scale preparations. This appeared to be due to elevated salt concentrations in combination with protein concentrations that were 2000–5000-fold higher than under the initial test conditions. High purity and integrity of the GlyR α1 fragments was verified by Coomassie gel staining (Fig. 3*A*) and Western blot analysis (Fig. 3*B*) using mAb4a for the extracellular domain and His-tag antibody for the intracellular domain. Mass spectrometry analysis by MALDI-TOF-MS and SELDI of pure protein constructs from *E. coli* verified the molecular weights of 12,115 kDa for the intracellular domain and 30,685 kDa for the N-terminal construct Sα1_(1–219) (Fig. 3*C*). All N-terminal constructs and the full-length receptor showed significant levels of expression in HEK293 cells (Fig. 3*B*).

*Membrane Association of the GlyR N-terminal Domain*—Lacking all the transmembrane domains present in GlyR subunits, one would expect the N-terminal domain to be stable in aqueous solution. Surprisingly, throughout all preparation steps of extracellular constructs, we observed a strong tendency toward precipitation. Therefore, low-salt buffer conditions were chosen to ensure stable protein solutions. Construct S_α1-(1–219) showed increased protein solubility as compared with construct α1-(1–219) (not shown), indicating a stabilizing effect of the N-terminal S-tag. Ionic detergents (SDS and desoxycholate) increased the solubility of the N-terminal domain, while non-ionic and zwitterionic detergents (Tween 20, Triton X-100, 3-[(3-Cholamidopropyl)dimethylammonio]-1-propanesulfonate CHAPS, octylglucoside or dodecylmaloside) had no detectable effect. The observation that the N-terminal domain was less soluble than expected, led to the assumption that protein aggregation and precipitation might be attributed to hydrophobic patches in this domain. To test for possible interactions between putative hydrophobic surface stretches of this domain and lipid membranes, we expressed the eukaryotic construct SP_α1-(1–219) in HEK293 cells. Cell homogenates were separated into soluble and membrane fractions, and probed for GlyR antigen by Western blot analysis. Unless prevented by strong membrane attachment, a membrane-directing signal peptide would be expected to cause secretion of the target protein into the extracellular medium. However, the

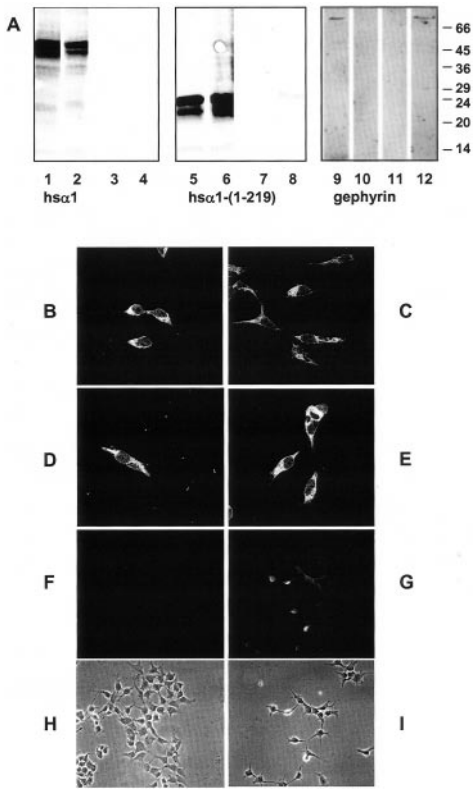


FIG. 4. **Membrane association of hsα1 and the N-terminal construct SP_α1-(1–219).** *A*, alkali extraction of HEK293 cell membranes transfected with hsα1 and SP_α1-(1–219) constructs. *Lane 1*, hsα1 pH 7.4, pellet; *lane 2*, hsα1 pH 11.0, pellet; *lane 3*, hsα1 pH 7.4, supernatant; *lane 4*, hsα1 pH 11.0, supernatant; *lane 5*, SP_α1-(1–219) pH 7.4, pellet; *lane 6*, SP_α1-(1–219) pH 11.0, pellet; *lane 7*, SP_α1-(1–219) pH 7.4, supernatant; *lane 8*, SP_α1 (1–219) pH 11.0, supernatant; *lane 9*, gephyrin pH 7.4, pellet; *lane 10*, gephyrin pH 11.0, pellet; *lane 11*, gephyrin pH 7.4, supernatant; *lane 12*, gephyrin pH 11.0, supernatant. *B–I*, immunocytochemistry (*B* and *C*) N-terminal domain SP_α1-(1–219); *D* and *E*, hsα1 wild-type. *F* and *G*, gephyrin. *H*, gephyrin, transmission image of fluorescence *photograph F*. *I*, gephyrin, transmission image of fluorescence *photograph G*. All images were taken in the absence (*B*, *D*, *F*, *H*) and presence (*C*, *E*, *G*, *I*) of Triton X-100.

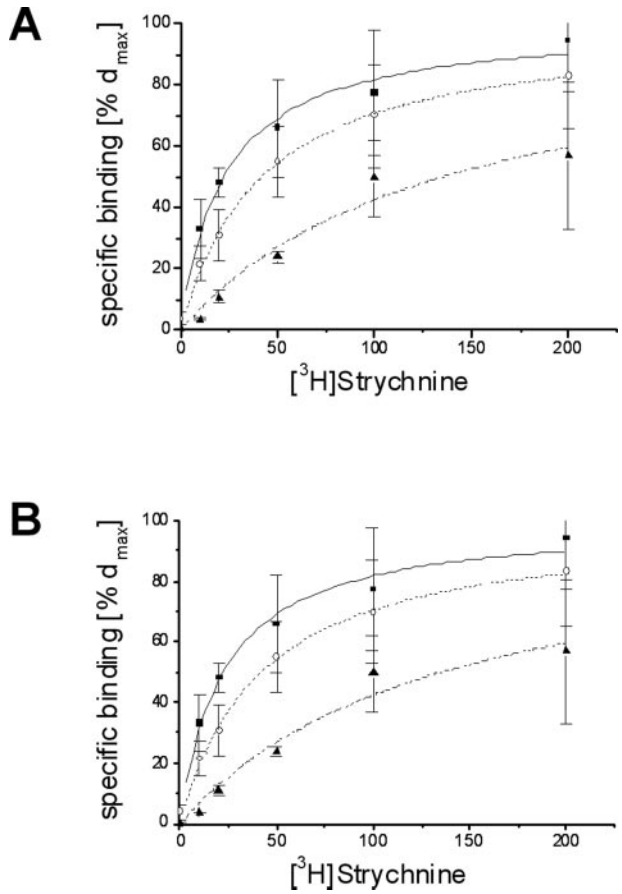


FIG. 5. **[$^3$H]Strychnine binding to GlyR α1 wild-type and N-terminal constructs.** *A*, total cell extract of transfected HEK293 cells: (■, *solid line*) wild type; (▲, *dashed line*) construct α1-(1–219); (○, *dotted line*) 6xHis_α1-(1–219). *B*, (■, *solid line*) hsα1 wild type, membrane preparation; (○, *dotted line*) SP_α1-(1–219), membrane preparation; (▲, *dashed line*) S_α1-(1–219), refolded from *E. coli*. $K_D$, and $B_{max}$ values are summarized in Table II.

immune signal of the construct SP_α1-(1–219) co-distributed exclusively with the membrane fraction, indeed indicative of a tight attachment. To check whether the N-terminal domain behaves like a peripheral or an integral membrane protein, we performed alkaline extraction experiments. Controls were made using the entire GlyR, and a coexpression of GlyR α1- and β-subunits, and gephyrin (1:4:4). While gephyrin could be extracted at alkaline pH, the entire GlyR remained in the membrane fraction as shown before (24) (Fig. 4*A*). Under these conditions the N-terminal domain SP_α1-(1–219) was found in the pellet at pH 7.4 and also at alkaline conditions (pH 11.0). Only minimal amounts of wild-type and truncated GlyR could be observed in the supernatant at pH 11.0 (Fig. 4*A*). This result would be expected for an integral membrane protein or a protein characterized by tight membrane association. To confirm this observation, the subcellular distribution of the SP_α1-(1–219) antigen was analyzed by immunocytochemistry. We hypothesized that an unspecific aggregation of the N-terminal domain inside the HEK293 cells, or its trapping in intracellular membranes, should restrict GlyR immune signals to the cell interior. However, immunostaining of HEK293 cells transfected with the N-terminal construct SP_α1-(1–219) showed a membrane distribution indistinguishable from the full-length α1 subunit. Additionally, permeabilization of transfected cells by Triton X-100 had no influence on immune signal distribution (Fig. 4, *B–E*). As control for an intracellular protein we chose gephyrin, which binds to the intracellular TM3–4 loop of the GlyR β subunit. HEK293 cells were cotransfected with GlyR α1, GlyR β, gephyrin (1:4:4) and probed with a gephyrin antibody. Here, the immune signal was only present in HEK293 cells that were permeabilized with Triton-X100 (Fig. 4, *F–I*). Taken together, these results consistently indicated a tight membrane association of the GlyR α1 extracellular domain, despite the complete absence of all putative transmembrane domains.

*High Affinity [$^3$H]Strychnine Binding of GlyR Extracellular Domains*—The N-terminal domain of the GlyR α1-subunit carries well characterized determinants of ligand binding. To analyze whether ligand binding was preserved in the truncated receptor subunit, we investigated various GlyR N-terminal constructs obtained from both, expression in HEK293 cells and refolded inclusion bodies. Efficient binding of [$^3$H]strychnine was observed for all of the constructs generated, yielding affinities similar to the wild type (Fig. 5). Total cell extracts, performed for constructs lacking the signal peptide, yielded apparent $K_D$ values of 115 ± 24 nM for the full-length GlyR, 107 ± 58 nM for construct α1-(1–219), and 66 ± 16 nM for construct His-α1-(1–219). Furthermore, membrane preparations were analyzed for the α1 wild-type construct and the membrane-associated construct SP_α1-(1–219), producing $K_D$ values of 23 ± 4 nM and 42 ± 3 nM, respectively, compared with a $K_D$ of 135 ± 67 nM for the refolded construct S_α1-(1–219). It should be noted that endogenous glycine could not be separated from the total cell extracts. Thus, the decrease in apparent affinity

TABLE II
*[$^3$H]strychnine binding to GlyR constructs*

| | hs$\alpha$1 | $\alpha$1-(1–219) | 6xHis-$\alpha$1-(1–219) | hs$\alpha$1 | SP-$\alpha$1-(1–219) | 6xHis-S-$\alpha$1-(1–219) |
|---|---|---|---|---|---|---|
| Expression | HEK293 | HEK293 | HEK293 | HEK293 | HEK293 | *E. coli* |
| Preparation | Total cell extract | Total cell extract | Total cell extract | Membrane preparation | Membrane preparation | Refolding |
| App $K_D$M] | 115 ± 24 | 107 ± 58 | 66 ± 16 | 23 ± 4 | 42 ± 3 | 135 ± 67 |
| $B_{max}$ [cpm][a] | 5511 ± 570 | 2163 ± 570 | 595 ± 58 | 8211 ± 418 | 308 ± 9 | 1383 ± 357 |
| Fig. 4 | A | A | A | B | B | B |

[a] $B_{max}$ under experimental conditions.

observed for these preparations as compared with membrane preparations, may be attributed to the endogenous amino acid agonist competing for [$^3$H]strychnine binding. However, when analyzed under identical conditions, the full-length GlyR $\alpha$1-subunit and the extracellular domain displayed similar $K_D$ values indicative of high affinity [$^3$H]strychnine binding (Table II).

*Oligomerization and Secondary Structure*—To study the oligomerization states of the isolated protein constructs from *E. coli*, we performed size exclusion chromatography under native conditions. Each GlyR-derived protein eluted in a single peak at high molecular weight that indicated oligomerization into complexes of defined stoichiometry. For construct S_$\alpha$1-(1–219), a molecular weight of ~464 kDa was observed (Fig. 6*B*), consistent with an association in the approximate range of 15 monomers. The apparent molecular weight of the cytosolic TM3–4 loop was determined to be ~49 kDa, compatible with a tetrameric arrangement (Fig. 6*A* and Table III). We were surprised by the high apparent molecular weight that was suggested by chromatography for the refolded N-terminal domain. Therefore, the GlyR N-terminal construct $\alpha$1-(1–219), expressed in HEK293 cells, was analyzed using a continuous 10–40% sucrose gradient. Here, a bimodal distribution of the N-terminal domain was obtained (Fig. 6*C*), providing apparent molecular masses of 124 and 378 kDa, which roughly corresponded to pentameric and 15-meric structures. These results were in good agreement with our molecular weight determination obtained by gel filtration.

With pure protein preparations, CD spectroscopy should permit a reliable estimate of the relative contribution of secondary structure elements, in particular of the $\alpha$-helical portion (28, 29). We recorded CD spectra of purified extra- and intracellular GlyR domains from *E. coli* to analyze the relative contribution of the secondary structure elements (Fig. 7). Constructs $\alpha$1-(1–219) and $\alpha$1-(309–392) contained a 16 residue stretch of His-tag plus thrombin site. In contrast, construct S_$\alpha$1-(1–219) additionally included an S-tag and factor Xa site, which resulted in a total of 50 amino acids before the target GlyR N-terminal domain. The $\alpha$-helical contribution was quantified using two independent single wavelength methods, indicating about 16% (29) or 24% (28) of $\alpha$-helix for the extracellular construct $\alpha$1-(1–219) and 15% (29) or 18% (28) for the construct S_$\alpha$1-(1–219). The lower $\alpha$-helical content in construct S_$\alpha$1-(1–219) as compared with construct $\alpha$1-(1–219) suggested that the additional sequence itself did not add significantly to the secondary structure. An estimation of $\alpha$-helical content by comparison of CD spectra with the reference data base of Yang *et al.* (30) was in agreement with the single wavelength methods used. While this method predicted a significant amount of $\beta$-sheet for the N-terminal domain, we turned to FTIR as the more appropriate technique for quantification of $\beta$ structures. The cytosolic TM3–4 loop on the other hand showed no detectable $\alpha$-helical structures. The CD spectra were indicative of the presence of a mixture of $\beta$-sheet and coil structures while the minimum around 203 nm strongly suggested the existence of a PPII helix, which has a minimum at 204 nm (26, 27). The stretch of amino acids ($^{365}$PPPAPSKSP$^{373}$) might be the likely candidate for this structural element.

We then assessed the secondary structure of the N-terminal domain of the GlyR $\alpha_1$ subunit S-$\alpha$1-(1–219) by FTIR spectroscopy. The frequencies of the amide I and II absorption bands which are primarily caused by peptide C = O and C-N stretching modes, respectively, are sensitive to the secondary structure of the peptide backbone. The amide I absorption in the 1620–1690 cm$^{-1}$ range is particularly informative with regard to types of secondary structure. Frequencies in the 1620–1640 cm$^{-1}$ and 1652–1660 cm$^{-1}$ range are typically associated with $\beta$-sheet and $\alpha$-helical structures, respectively, whereas random structures mainly absorb between 1640 and 1650 cm$^{-1}$. Here, we followed the assignments given in the literature (31–33). Amide I and II absorption bands of the N-terminal extracellular domain S-$\alpha$1-(1–219) at pH 7.4 (Fig. 7*B*, *trace b*) showed distinct minima in the second derivative of the absorption spectrum (Fig. 7*B*, *trace a*). These indicated the presence of different underlying populations of amide I modes near 1626, 1646, 1655, 1680, and 1692 cm$^{-1}$, which gave rise to the asymmetry as well as the discernable shoulders in the amide I contour of the expressed receptor domain. In agreement with this identification of underlying components, the amide I band was fitted with five gaussian components corresponding to the center frequencies from the second derivative minima. Based on the band integrals, the analysis of the FTIR spectra suggests a secondary structure composition of 25% $\alpha$-helices, 48% $\beta$-sheets, 17% $\beta$-turns, and 10% random structure. In an analogous investigation of the secondary structure of the GlyR TM3–4 loop, gaussian bands could again be fitted that agreed well with the positions identified by the second derivative spectrum (Fig. 7*C*). The prominent gaussian component is centered at 1650 cm$^{-1}$, a frequency that is difficult to assign because it falls between the typical frequencies of absorption by $\alpha$-helices above 1650 cm$^{-1}$ and of "random coils" below 1650 cm$^{-1}$. The second largest band is located at 1675 cm$^{-1}$, indicative of $\beta$-turns. The band at 1632 cm$^{-1}$ agrees with $\beta$-sheet structure, whereas the lowest frequency band at 1616 cm$^{-1}$ cannot be assigned to a classical secondary structure. In summary, the TM3–4 loop peptide appears to contain roughly 20% $\beta$-sheet structure and 30% $\beta$-turns but is probably less ordered than the N-terminal extracellular domain and has less, if any, $\alpha$-helical content. The results are summarized and compared with data found in the literature in Table IV.

## DISCUSSION

The inhibitory GlyR is a member of the acetylcholine receptor superfamily. Each of its subunits consists of an extracellular domain, four transmembrane regions, and a large cytosolic TM3–4 loop. Here, the GlyR $\alpha$1 extramembraneous domains were generated and expressed in *E. coli* and eukaryotic HEK293 cells. The isolated eukaryotic and refolded extracellular domain retained its characteristic high affinity

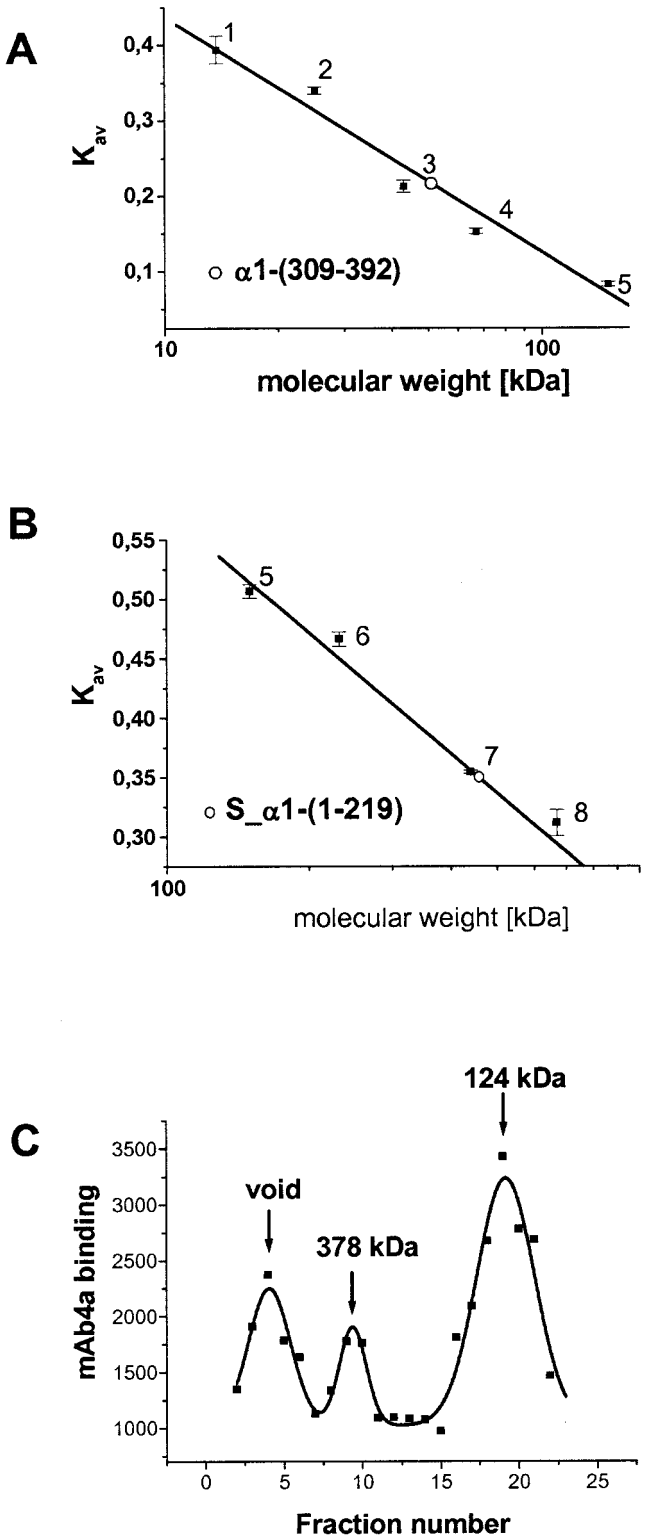


FIG. 6. **Determinations of native molecular weight of GlyR constructs.** For chromatography, marker proteins were (1) ribonuclease A, 13.7 kDa; (2) chymotrypsinogen A, 25 kDa; (3) ovalbumin, 43 kDa; (4) albumin, 67 kDa; (5)γ-globulin, 150 kDa; (6) catalase (232 kDa); (7) ferritin, (440 kDa); (8) thyroglobulin (669 kDa). Mean $K_{av}$ ± S.D. of the calibration proteins from triplicate determinations are plotted. *A*, intracellular loop α1-(309–392), Sephacryl S200 column, $MW_{app}$ = 49 ± 1 kDa. *B*, extracellular domain α1-(1–219), Sephacryl S400 column, $MW_{app}$ = 465 ± 33 kDa. *C*, sucrose gradient centrifugation. A 10–40% sucrose gradient was used and GlyR antigen visualized by DORA. Apparent molecular weights are indicated. See Table III for results.

TABLE III
*Oligomerization of GlyR extramembraneous domains*

| Construct | MW monomer calculated | MW determined | Method |
|---|---|---|---|
| | *kDa* | *kDa* | |
| α1-(309–392) (No. 6) | 12.1 | 49 ± 1 | Size exclusion Chr. |
| *S*-α1-(1–219) (No. 2) | 30.7 | 465 ± 33 | Size exclusion Chr. |
| HEK-α1-(1–219) (No. 3) | 25.4 | 378<br>124 | Sucrose gradient |

[$^3$H]strychnine binding and, unexpectedly, showed a strong membrane attachment. Secondary structure analysis suggested a significant contribution of α-helices to the N-terminal domain, while no α-helical structure was found in the cytosolic TM3–4 loop.

Following expression in *E. coli*, the large intracellular loop α1-(309–392) was purified under native conditions. Due to inclusion body formation, the extracellular constructs α1-(1–219) and S_α1-(1–219) were refolded after denaturation. While low solubility was a characteristic property of these refolded N-terminal constructs, the additional N-terminal S-tag reduced, but did not prevent, precipitation of the purified protein. This pronounced instability in solution suggested the presence of considerable hydrophobic surface areas, mediating protein aggregation. Thus the isolated N-terminal domain would be expected to show tight membrane association. Indeed, membrane preparation of the construct SP_α1-(1–219) from transfected HEK293 cells, followed by Western blot analysis, confirmed this prediction: the immune signal of the extracellular domain was exclusively co-distributed with the membrane, but not with the soluble fraction. Even at alkaline conditions (pH 11.0) the N-terminal domain SP_α1-(1–219) remained with the membrane fraction. In fact, the entire GlyR and the N-terminal domain showed practically identical behavior under the condition of alkaline extraction, indicating a very tight membrane association of the isolated N-terminal domain. Although this observation may be compatible with an association of the isolated N-terminal domain with the plasma membrane, we could not exclude an association with intracellular membranes or an unspecific precipitation within the cytosol yielding the same result. To further elucidate the subcellular localization of the isolated GlyR N-terminal domain, we performed immunocytochemistry experiments in transfected HEK293 cells. The subcellular distribution of the isolated N-terminal domain was indistinguishable from that of the full-length α1-subunit, confirming its attachment to the plasma membrane. The pronounced tendency toward precipitation as well as a strong membrane attachment of the GlyRα1 N-terminal domain were consistent with the presence of hydrophobic surface areas, as previously proposed from studies of reconstituted GlyRs (19). When the extracellular domain of the α7 nAChR was expressed in *E. coli* as an isolated refolded protein (13), solubility was likewise reduced. Thus, significant hydrophobic interaction stretches within the extracellular domain appear to be a property of many members of the acetylcholine receptor superfamily.

High affinity strychnine binding is an important functional characteristic of the inhibitory GlyR (2). Indeed, we observed identical [$^3$H]strychnine affinities for the full-length α1-subunit and the isolated N-terminal domains from HEK293 cell preparations. High affinity strychnine binding persisted even in the refolded isolated protein from *E. coli* expression, with an affinity reduced only 3–6-fold compared with the full-length receptor. These observations indicated a proper folding of the extracellular domain into its functional conformation, independent of other extracellular or transmembrane

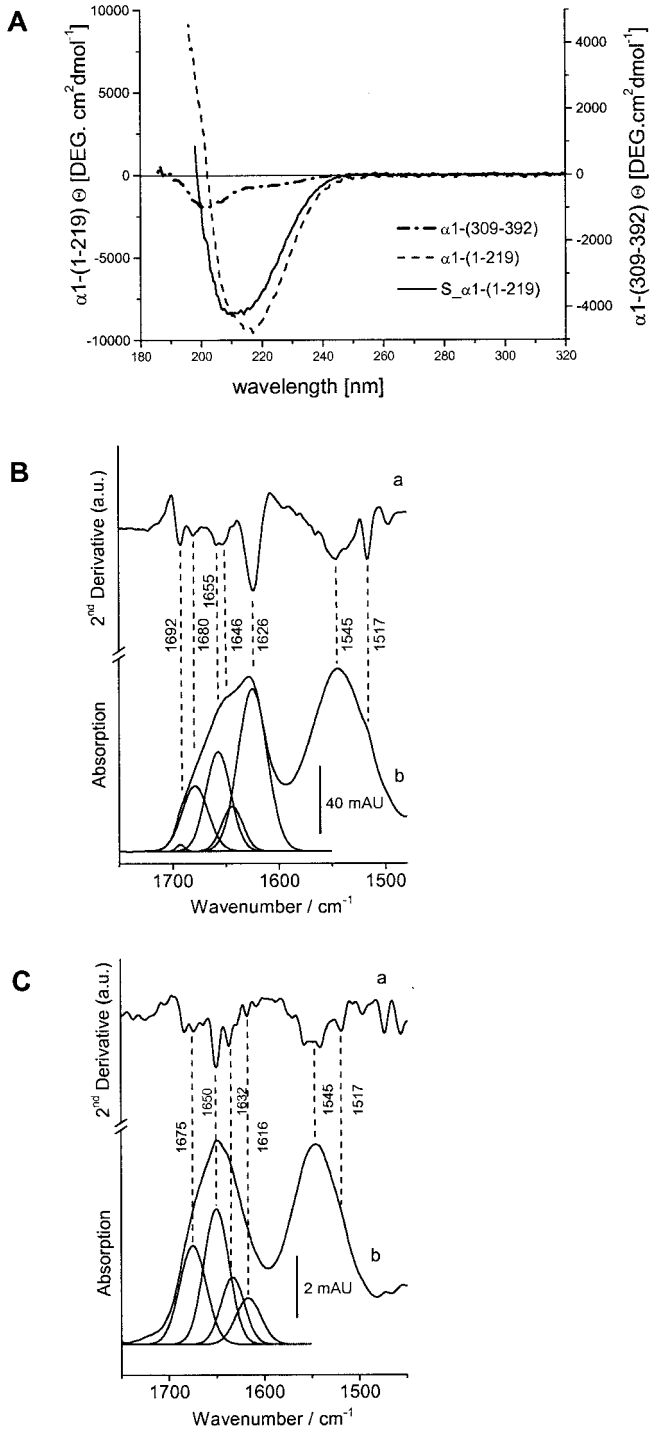


FIG. 7. **Secondary structure determination.** *A*, CD spectra of intra- and extracellular domains of the glycine receptor. The spectra are baseline corrected and represent the average of 8 individual scans. Proteins were buffered in 10 mM potassium phosphate, pH 7.4. Scans were taken at 0.5-nm intervals in a 0.1-cm pathlength cell. *B*, FTIR-based secondary structure analysis of the GlyR extracellular domain measured in 10 mM sodium phosphate buffer pH 7.4. *a*, second derivative of the IR-absorption spectrum in the amide I and II frequency range. Negative bands indicate the peak positions of underlying absorption bands. *b*, gaussian bands obtained from a fit of the amide I absorption. *C*, FTIR-based secondary structure analysis of the GlyR TM3–4 loop measured in 10 mM sodium phosphate buffer, pH 7.4. *a*, second derivative of the IR-absorption spectrum in the amide I and II frequency range. Negative bands indicate the peak positions of underlying absorption bands. *b*, gaussian bands obtained from a fit of the amide I and II absorption using the OPUS software. For clarity, only the bands in the amide I range are shown.

regions. Similar conservation of wild-type-like ligand affinity was observed with the N-terminal domain of chicken α7 nAChR expressed in *Xenopus* oocytes (10). In contrast, when the nAChR extracellular domain fused to maltose-binding protein is expressed in *E. coli*, ligand affinity is reduced 1000-fold, as compared with full-length nAChR (11). Furthermore, affinity for α-bungarotoxin of the refolded α7 AChR extracellular domain expressed in *E. coli* and of muscle AChR N-terminal domain expressed in yeast is reduced 10- to 1000-fold (12, 13, 36). With a ligand binding affinity approaching that of the complete α1-subunit, the refolded GlyR extracellular domain apparently had reached a high degree of structural integrity.

Behavior of the full-length GlyR α1-subunit during sucrose gradient centrifugation is compatible with a pentameric association (22, 37). Likewise, molecular weight determination of the GlyR extracellular constructs by size exclusion chromatography revealed a multisubunit assembly. As the hydrodynamic volume of a protein depends on both, its mass and its surface properties, the molecular weight values obtained represent only estimates. Despite these limitations, the apparent molecular weights determined for the cytosolic TM3–4 loop and the truncated extracellular protein would be compatible with tetrameric and 15-meric complexes, respectively. When the N-terminal domain solubilized from HEK293 cells was investigated on sucrose gradients, a bimodal molecular weight distribution suggested multimers of about 5 and 15 subunits. As determinants directing α-subunit assembly are situated within the GlyR N-terminal domain (16), pentameric agglomeration would indeed be expected for the isolated extracellular domain, rather than for the TM3–4 loop. Taken together, our data for the N-terminal domain were in good agreement with the expected pentameric association (4, 22, 37). In contrast, tetrameric association of the isolated TM3–4 loop remains unexplained, but may be attributed to an intracellular interaction site of GlyR subunits.

To investigate secondary structure elements within the isolated extramembraneous domains expressed in *E. coli*, we performed circular dichroism (CD) and Fourier transform infrared (FTIR) spectroscopy studies. Spectra taken of the TM3–4 loop α1-(309–392) suggested no α-helical portion at all. While CD and FTIR investigation both predicted significant amounts of β-structure, the distinct CD maximum at 203 nm indicated the formation of a PPII helix. It should be noted that the TM3–4 loop cannot be tested for its functional reconstitution. This implies, that a folding of the intracellular domain in the holoreceptor protein different from that in the isolated state cannot be excluded. However, the distinct spectral signal of a PPII helix, which is also present in the entire reconstituted GlyR protein (41), suggested a correct folding of the prominent secondary structure elements. In contrast, data obtained for construct α1-(1–219) predicted an α-helical content of 24% (CD, 208 nm, Ref. 28) while spectra obtained from construct S_α1-(1–219) pointed to 18% (CD, 208 nm) or 25% (FTIR) α-helices (Table IV). CD and FTIR spectra further indicated significant amounts of β-sheet in the extracellular domain (48% by FTIR investigation), in good agreement with values found for the acetylcholine binding protein (14) and AChR extracellular domains (Table IV). However, low α-helical contents of 8% were found for the AChBP from *Lymnaea stagnalis* (14), and 12–14% for soluble, monomeric preparations of mouse muscle nAChR N-terminal domains (38, 39). In contrast, preparations of rat α7 and Torpedo N-terminal AChR domains, both forming oligomeric assemblies, showed α-helical contents of 32–44% (13, 36). Even within the AChR family, extracellular domains from

TABLE IV
*Secondary structure assignments*

| Protein | Method | α-Helix | β-Sheet | β-turn | Rand. coil | PPII helix | Ref. |
|---|---|---|---|---|---|---|---|
| | | % | % | % | % | % | |
| α1-(1–219) GlyR | CD | 24[a] | +[b] | n.d.[c] | n.d. | −[d] | This study |
| *S*-α1-(1–219) GlyR | CD | 18[a] | + | n.d. | n.d. | − | |
| *S*-α1-(1–219) GlyR | FTIR | 25 | 48 | 17 | 10 | n.d. | |
| α1-(309–392) GlyR | CD | 0[a] | + | n.d. | n.d. | + | |
| α1-(309–392) GlyR | FTIR | 0 | ca. 20 | ca. 30 | n.d. | n.d. | |
| α1 GlyR *Homo sapiens* | CD | 15 | 37 | 22 | 18 | 9 | (41) |
| α-(1–210) nAChR *Mouse muscle* | CD | 12<br>14[a] | 51 | 18 | 20 | | (38) |
| α-(1–211) nAChR *Mouse muscle* | CD | 14 | 46 | 21 | 19 | | (39) |
| GST-α7 (1–208) nAChR *rat* | CD | 43–44 | 12–27 | | 29–45 | | (13) |
| α(1–209) nAChR *Torpedo california* | CD | 32–35[e] | 50–56[e] | 0–8[e] | 10[e] | | (36) |
| AChBP *Lymnaea stagnalis* | Crystal structure | 8 | 47 | | | | (14) |
| nAChR *Torpedo nobiliana* | CD | 34 | 29 | | | | (43) |
| nAChR | Raman | 35 | 33 | | | | (44) |
| nAChR *Torpedo californica* | CD | 23 | 43 | 6 | 28 | | (45) |
| nAChR *Torpedo californica* | CD | 40 | 20 | 10 | 30 | | (46) |
| nAChR *Torpedo* | FTIR | 39 | 35 | 6 | 20 | | (47) |

[a] After Ref. (28).
[b] +, present, not quantified (see text).
[c] n.d., not determined.
[d] −, no corresponding signals detected.
[e] Dependent on expression vector

different sources appear to contain varying amounts of secondary structure elements. As evident from comparison with other protein constructs, the His-tag present in the GlyR constructs is unlikely to contribute to or induce α-helical motifs (49). Secondary structure assignments of the entire receptor protein show relative α-helical contents of 23–40% for *Torpedo* nAChR, and only ~15% for the GlyR (Table IV). For the GlyR N-terminal domain, the α-helical content was low compared with the *Torpedo* nAChR, but higher than the amount of α-helix found for the muscle nAChR, or the acetylcholine binding protein. As the GlyR extracellular domain accounts for ca. 50% of the total protein, the α-helical content of about 25% derived from our CD and FTIR- data would correspond to a portion of about 12% of the full-length α1 subunit. Given that the helical structure of TM2 (8, 9, 15, 40) contributes a further 5%, a total of at least 17% α-helical structure would be expected for the entire GlyR α1 subunit. This is in qualitative agreement with the prediction of about 15% α-helical content for the reconstituted GlyR α1-subunit (41) or its fragment α1-(165–291) (42). This would suggest that not all transmembrane domains of the GlyR are α-helical, and is consistent with the absence of α-helices in the TM3–4 loop.

Our results show high affinity strychnine binding for the eukaryotic and refolded N-terminal domains. Interestingly, the isolated extracellular domain showed a strong membrane association when expressed in HEK293 cells, indicating that hallmarks of holoreceptor structure are indeed conserved in the isolated N-terminal domain.

*Acknowledgments*—We thank Prof. Paul Rösch for use of the CD spectrometer, Prof. Heinrich Sticht and Dr. Carmen Villmann for helpful discussions and a critical reading of the manuscript, Drs. Claus Stolt, Andreas Humeny, and Silke Seeber for help with fluorescence microscopy and mass spectroscopy, and Rosa Weber for cell culture and maintenance.

REFERENCES

1. Schofield, P. R., Lynch, J. W., Rajendra, S., Pierce, K. D., Handford, C. A., and Barry, P. H. (1996) *Cold Spring Harb. Symp. Quant. Biol.* **61,** 333–342
2. Breitinger, H.-G., and Becker, C.-M. (1998) *Curr. Pharm. Des.* **4,** 315–334
3. Becker, K., Becker, C.-M., and Breitinger, H.-G. (2000) in *Channelopathies* (Lehmann-Horn, F., ed), pp. 199–224, Elsevier, Amsterdam, NL
4. Langosch, D., Thomas, L., and Betz, H. (1988) *Proc. Natl. Acad. Sci. U. S. A.* **85,** 7394–7398
5. Hucho, F., and Weise, C. (2001) *Angew. Chem. Int. Ed.* **40,** 3100–3116
6. Laube, B., Maksay, G., Schemm, R., and Betz, H. (2002) *Trends Pharmacol. Sci.* **23,** 519–527
7. Betz, H. (1990) *Neuron* **5,** 383–392
8. Opella, S. J., Marassi, F. M., Gesell, J. J., Valente, A. P., Kim, Y., Oblatt-Montal, M., and Montal, M. (1999) *Nat. Struct. Biol.* **6,** 374–379
9. Tang, P., Mandal, P. K., and Xu, Y. (2002) *Biophys. J.* **83,** 252–262
10. Wells, G. B., Anand, R., Wang, F., and Lindstrom, J. (1998) *J. Biol. Chem.* **273,** 964–973
11. Fischer, M., Corringer, P. J., Schott, K., Bacher, A., and Changeux, J. P. (2001) *Proc. Natl. Acad. Sci. U. S. A.* **98,** 3567–3570
12. Psaridi-Linardaki, L., Mamalaki, A., Remoundos, M., and Tzartos, S. J. (2002) *J. Biol. Chem.* **277,** 26980–26986
13. Tsetlin, V. I., Dergousova, N. I., Azeeva, E. A., Kryukova, E. V., Kudelina, I. A., Shibanova, E. D., Kasheverov, I. E., and Methfessel, C. (2002) *Eur. J. Biochem.* **269,** 2801–2809
14. Brejc, K., van Dijk, W. J., Klaassen, R. V., Schuurmans, M., van Der Oost, J., Smit, A. B., and Sixma, T. K. (2001) *Nature* **411,** 269–276
15. Unwin, N. (1996) *J. Mol. Biol.* **257,** 586–596
16. Breitinger, H.-G., and Becker, C.-M. (2002) *ChemBioChem.* **3,** 1042–1052
17. Griffon, N., Buttner, C., Nicke, A., Kuhse, J., Schmalzing, G., and Betz, H. (1999) *EMBO J.* **18,** 4711–4721
18. Grenningloh, G., Rienitz, A., Schmitt, B., Methfessel, C., Zensen, M., Beyreuther, K., Gundelfinger, E. D., and Betz, H. (1987) *Nature* **328,** 215–220
19. Cascio, M. (2002) *Biopolymers* **66,** 359–368
20. Chen, G. Q., and Gouaux, E. (1997) *Proc. Natl. Acad. Sci. U. S. A.* **94,** 13431–13436
21. Heiring, C., and Muller, Y. A. (2001) *Protein Eng.* **14,** 183–188
22. Sontheimer, H., Becker, C.-M., Pritchett, D. B., Schofield, P. R., Grenningloh, G., Kettenmann, H., Betz, H., and Seeburg, P. H. (1989) *Neuron* **2,** 1491–1497
23. Kling, C., Koch, M., Saul, B., and Becker, C.-M. (1997) *Neuroscience* **78,** 411–417
24. Schmitt, B., Knaus, P., Becker, C.-M., and Betz, H. (1987) *Biochemistry* **26,** 805–811
25. Brahms, S., and Brahms, J. (1980) *J. Mol. Biol.* **138,** 149–178
26. Greenfield, N. J. (1996) *Anal. Biochem.* **235,** 1–10
27. Schweimer, K., Hoffmann, S., Bauer, F., Friedrich, U., Kardinal, C., Feller, S. M., Biesinger, B., and Sticht, H. (2002) *Biochemistry* **41,** 5120–5130
28. Greenfield, N., and Fasman, G. D. (1969) *Biochemistry* **8,** 4108–4116
29. Scholtz, J. M., Qian, H., York, E. J., Stewart, J. M., and Baldwin, R. L. (1991) *Biopolymers.* **31,** 1463–1470
30. Yang, J. T., Wu, C. S., and Martinez, H. M. (1986) *Methods Enzymol.* **130,** 208–269
31. Bandekar, J. (1992) *Biochim. Biophys. Acta* **1120,** 123–143
32. Dong, A., Huang, P., and Caughey, W. S. (1990) *Biochemistry* **29,** 3303–3308
33. Krimm, S., and Bandekar, J. (1986) *Adv. Protein. Chem.* **38,** 181–364
34. Breitinger, H.-G., Villmann, C., Becker, K., and Becker, C.-M. (2001) *J. Biol. Chem.* **276,** 29657–29663
35. Rudolph, R., and Lilie, H. (1996) *Faseb J.* **10,** 49–56
36. Alexeev, T., Krivoshein, A., Shevalier, A., Kudelina, I., Telyakova, O., Vincent, A., Utkin, Y., Hucho, F., and Tsetlin, V. (1999) *Eur. J. Biochem.* **259,** 310–319
37. Pfeiffer, F., Graham, D., and Betz, H. (1982) *J. Biol. Chem.* **257,** 9389–9393
38. West, A. P., Jr., Bjorkman, P. J., Dougherty, D. A., and Lester, H. A. (1997) *J. Biol. Chem.* **272,** 25468–25473
39. Yao, Y., Wang, J., Viroonchatapan, N., Samson, A., Chill, J., Rothe, E., Anglister, J., and Wang, Z. Z. (2002) *J. Biol. Chem.* **277,** 12613–12621
40. Unwin, N. (1995) *Nature* **373,** 37–43
41. Cascio, M., Shenkel, S., Grodzicki, R. L., Sigworth, F. J., and Fox, R. O. (2001)

*J. Biol. Chem.* **276,** 20981–20988
42. Xue, H., Shi, H., Tsang, S. Y., Zheng, H., Savva, C. G., Sun, J., and Holzenburg, A. (2001) *J. Mol. Biol.* **312,** 915–920
43. Moore, W. M., Holladay, L. A., Puett, D., and Brady, R. N. (1974) *FEBS Lett.* **45,** 145–149
44. Yager, P., Chang, E. L., Williams, R. W., and Dalziel, A. W. (1984) *Biophys. J.* **45,** 26–28
45. Mielke, D. L., and Wallace, B. A. (1988) *J. Biol. Chem.* **263,** 3177–3182
46. Wu, C. S., Sun, X. H., and Yang, J. T. (1990) *J. Protein Chem.* **9,** 119–126
47. Methot, N., McCarthy, M. P., and Baenziger, J. E. (1994) *Biochemistry* **33,** 7709–7717
48. Gill, S., and Hippel, P. (1989) *Anal. Biochem.* **182,** 319–326
49. Fletcher, C. M., Pestova, T. V., Hellen, C. U., and Wagner, G. (1999) *EMBO J.* **18,** 2631–2637